

Tissue Compartment	Age group (month)	Wild Type (N=11)		rTg-DI (N=10)		Diff	SE	P-value	L95%	U95%
		Mean mm <sup>3</sup>	SE	Mean mm <sup>3</sup>	SE					
Gray Matter Volume (mm <sup>3</sup> )	3	1137.2	9.8	1124.6	12.3	-12.7	15.7	0.430	-45.4	20.1
	6	1108.5	11.1	1123.1	9.8	14.6	14.7	0.334	-16.2	45.4
	9	1083.0	10.9	1086.1	13.6	3.1	17.4	0.861	-33.2	39.4
	11	1077.7	11.4	1080.4	12.0	2.7	16.6	0.872	-31.8	37.3
White Matter Volume (mm <sup>3</sup> )	3	554.4	5.8	531.6	8.7	-22.8	10.5	0.042	-44.6	-0.9
	6	603.3	6.5	590.1	9.0	-13.3	11.1	0.244	-36.3	9.8
	9	601.2	6.0	549.5	8.1	-51.7	10.1	<b>&lt;0.001</b>	-72.7	-30.7
	11	605.8	6.9	531.2	7.5	-74.5	10.1	<b>&lt;0.001</b>	-95.7	-53.4
Cerebral Spinal Fluid Volume (mm <sup>3</sup> )	3	260.2	6.1	247.5	5.3	-12.7	8.1	0.131	-29.5	4.1
	6	278.2	6.6	264.0	4.8	-14.2	8.1	0.096	-31.1	2.7
	9	258.0	5.5	267.8	5.6	9.8	7.9	0.229	-6.6	26.1
	11	251.3	6.2	289.6	6.7	38.3	9.1	<b>&lt;0.001</b>	19.2	57.3
Total Intracranial (mm <sup>3</sup> )	3	1951.8	18.1	1903.7	20.8	-48.1	27.6	0.096	-105.6	9.4
	6	1990.1	19.3	1977.2	21.7	-12.9	29.1	0.663	-73.5	47.8
	9	1942.2	19.1	1903.4	20.6	-38.9	28.0	0.181	-97.3	19.6
	11	1934.8	20.8	1901.3	19.9	-33.6	28.8	0.257	-93.6	26.5

**Supplementary Table 1: Summary of volumetric tissue compartment changes in WT and rTg-DI rats**

Data are presented as means and SE's Generalized Estimating Equations (GEE). Mean differences compare rTg-DI vs WT groups at each age group.

Age group midpoints* (month)	Wild Type		rTg-DI		Diff	SE	P-value	L95%
	Mean FA	SE	Mean FA	SE				
3.28 ± 0.19	0.370	0.003	0.368	0.002	-0.003	0.004	0.421	-0.010
6.23 ± 0.50	0.377	0.004	0.369	0.004	-0.009	0.005	0.114	-0.019
8.22 ± 0.45	0.387	0.003	0.378	0.002	-0.010	0.004	<b>0.010</b>	-0.017
11.33 ± 0.55	0.402	0.002	0.375	0.002	-0.026	0.002	<b>&lt;0.001</b>	-0.031

**Supplementary Table 2: Summary of FA changes in white matter compartment in WT and rTg-DI rats**

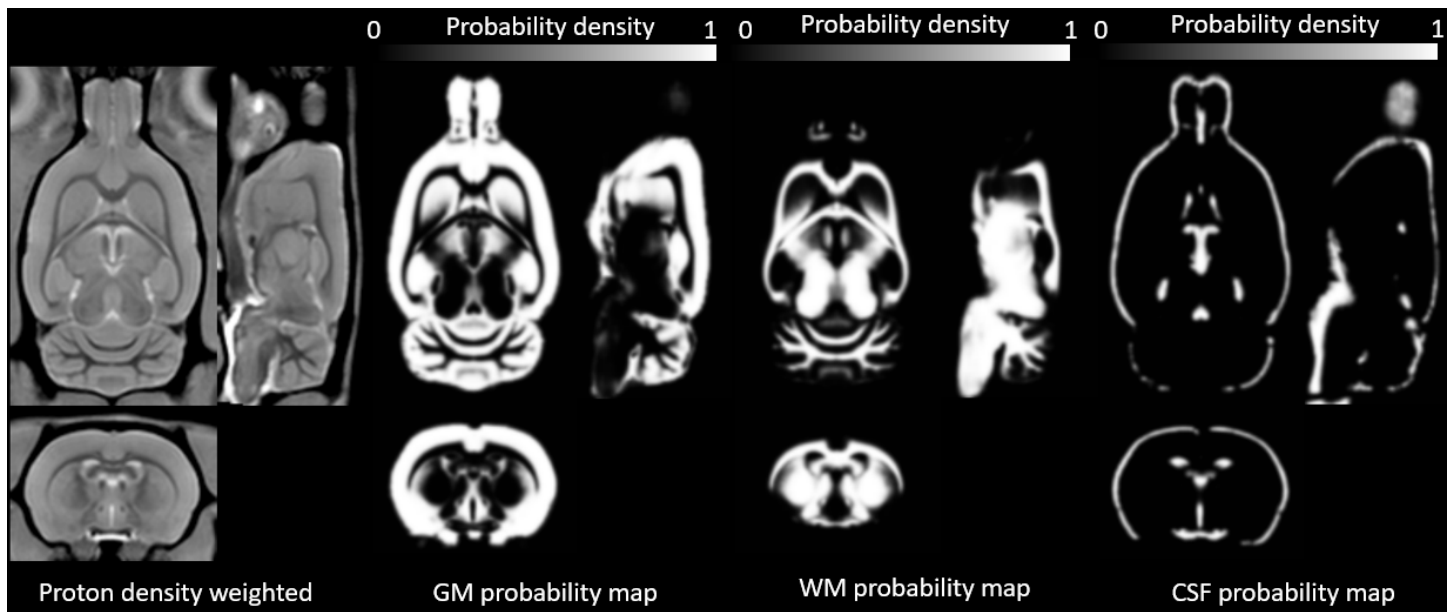
Data are presented as means and SE's Generalized Estimating Equations (GEE). Pairwise comparisons between the two strains at each age were investigated. The p-values were not adjusted for multiple comparisons

\*The age categories for statistical analysis comparison of FA values between the two strains are listed. These age groupings were used for the statistical analysis as well as for the voxel-wise analysis. The number of rats and gender distribution for each age group are as follows: 3 month groups: WT, N=7 (7 Females, 0 Males); rTg-DI, N=7 (7 Females, 0 Males); 6 month groups: WT, N=15 (11 Females, 4 Males); rTg-DI, N=14 (11 Females, 3 Males); 8 month groups: WT, N=10 (9 Females, 1 Male); rTg-DI, N=10 (8 Females, 2 Males); 11 month groups: WT, N=12 (10 Females, 2 Males); rTg-DI, N=13 (11 Females, 2 Males).

		Wild Type (N=11)		rTg-DI (N=10)						
Parameter	Age group (month)	Mean	SE	Mean	SE	Diff	SE	P-value	L95%	U95%
T2* Thalamus (ms)	3	28.9	0.20	28.9	0.26	0.01	0.33	0.988	-0.7	0.7
	6	29.6	0.32	27.8	0.30	-1.8	0.44	<b>0.001</b>	-2.7	-0.9
	9	28.8	0.36	25.9	0.25	-2.9	0.44	<b>&lt;.001</b>	-3.8	-2.0
	11	28.4	0.24	25.4	0.17	-3.0	0.29	<b>&lt;.001</b>	-3.6	-2.4
Thalamic Microbleed Volume (mm <sup>3</sup> )	3	0.61	0.076	0.80	0.130	0.19	0.150	0.229	-0.13	0.50
	6	0.43	0.101	1.27	0.294	0.84	0.311	<b>0.013</b>	0.19	1.49
	9	0.47	0.118	4.90	0.543	4.43	0.556	<b>0.000</b>	3.27	5.59
	11	0.76	0.121	6.96	0.448	6.20	0.464	<b>0.000</b>	5.23	7.17

### Supplementary Table 3: Summary of T2\* Microbleed Volume changes WT and rTg-DI rats

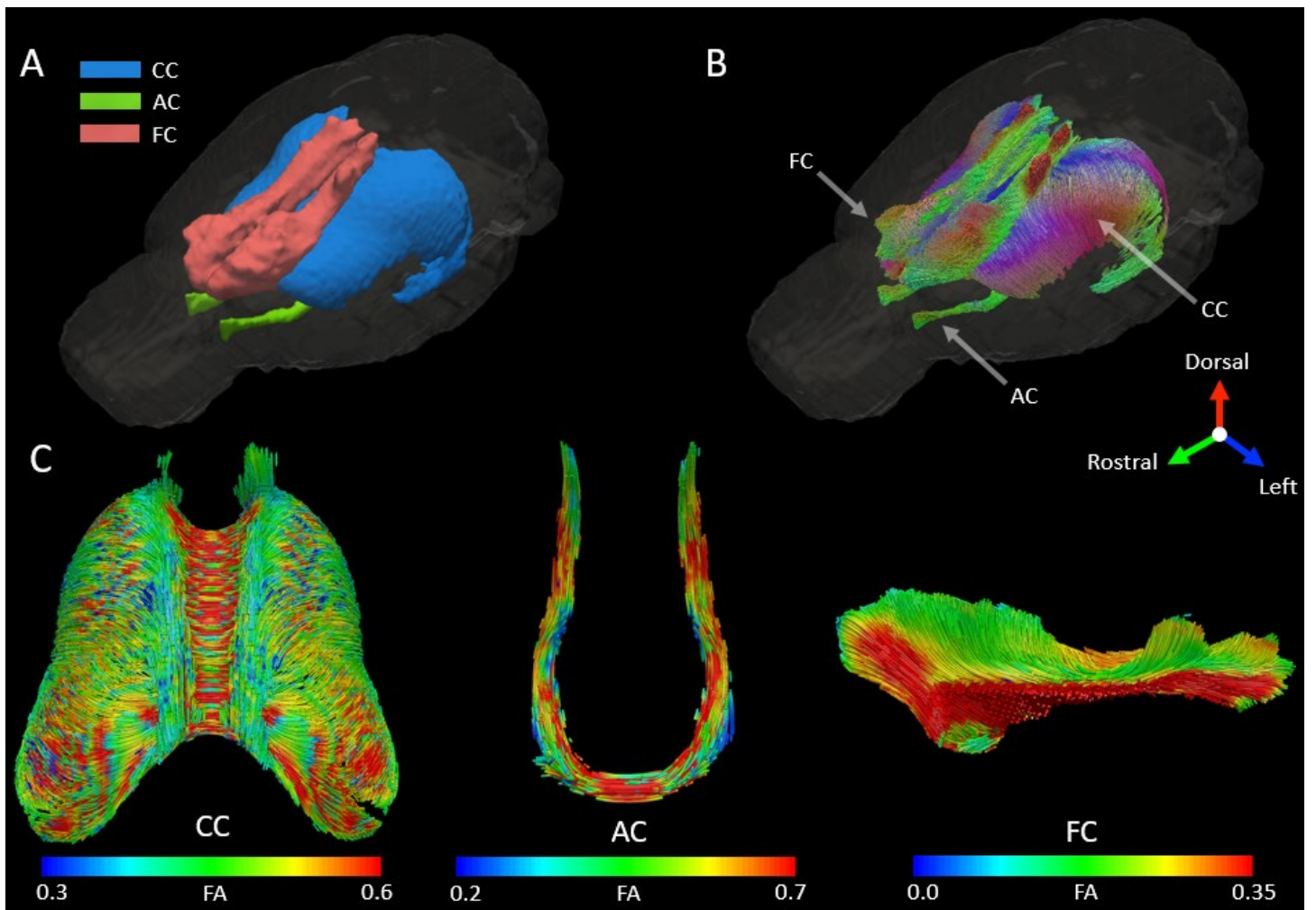
Data are presented as means and SE's Generalized Estimating Equations (GEE). Pairwise comparisons between the two strains at each age were investigated. The p-values were not adjusted for multiple comparisons



### Supplementary Figure 1: Population averaged proton density weighted images and tissue probability maps

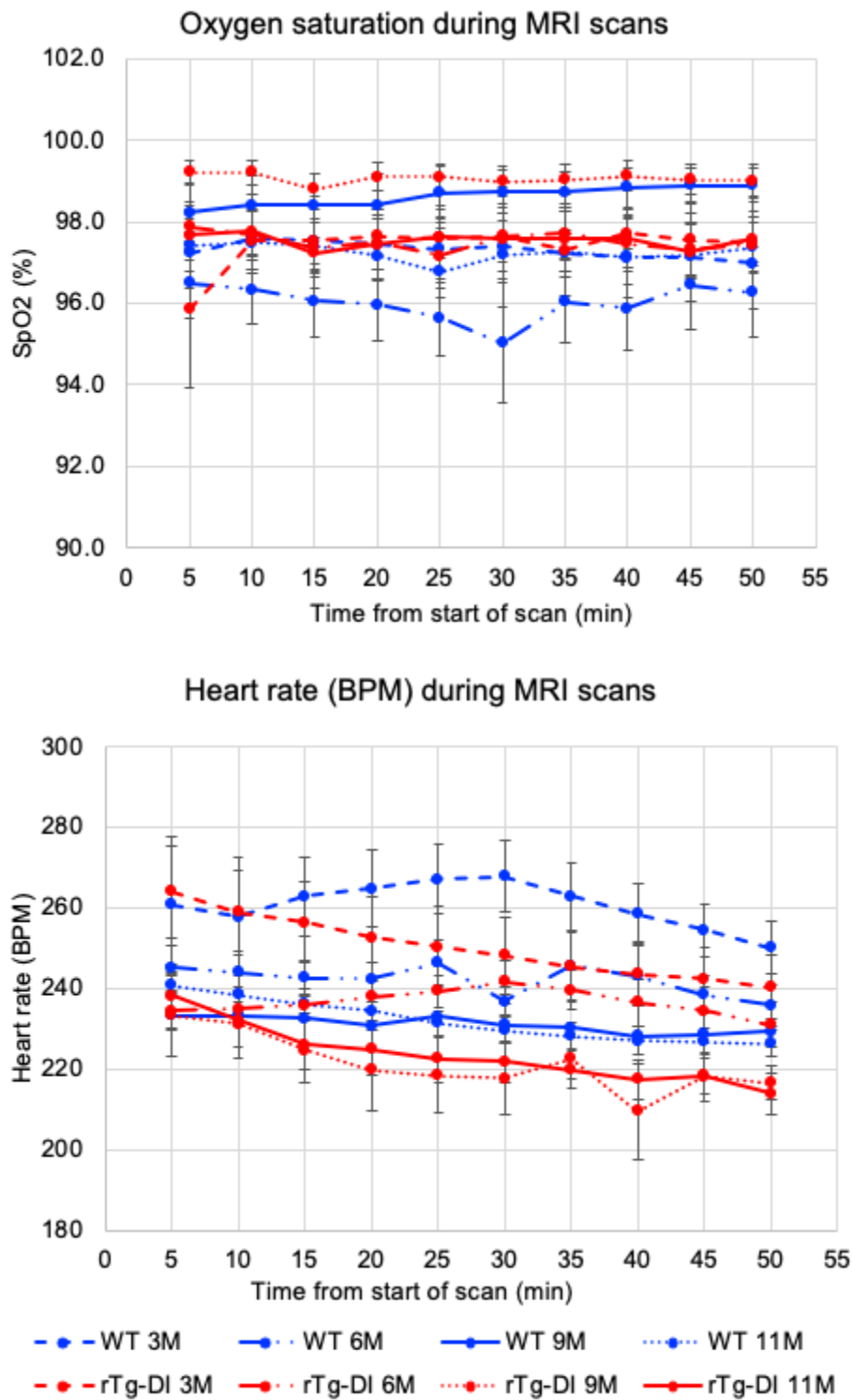
Voxel-based morphometry (VBM) was performed using custom made rTg-DI tissue probability maps (tpms). A total of 54 proton density weighted (PDW) scans (11 WT and 10 rTg-DI acquired at 4 time points) without conspicuous microbleeds were segmented, registered and population averaged using the unified segmentation

method and DARTEL registration algorithm. The initial rTg-DI tpms were constructed by segmenting the PDW images using the publicly available Wistar tpms followed by manual editing to improve the accuracy as described in (Koundal et.al 2019).

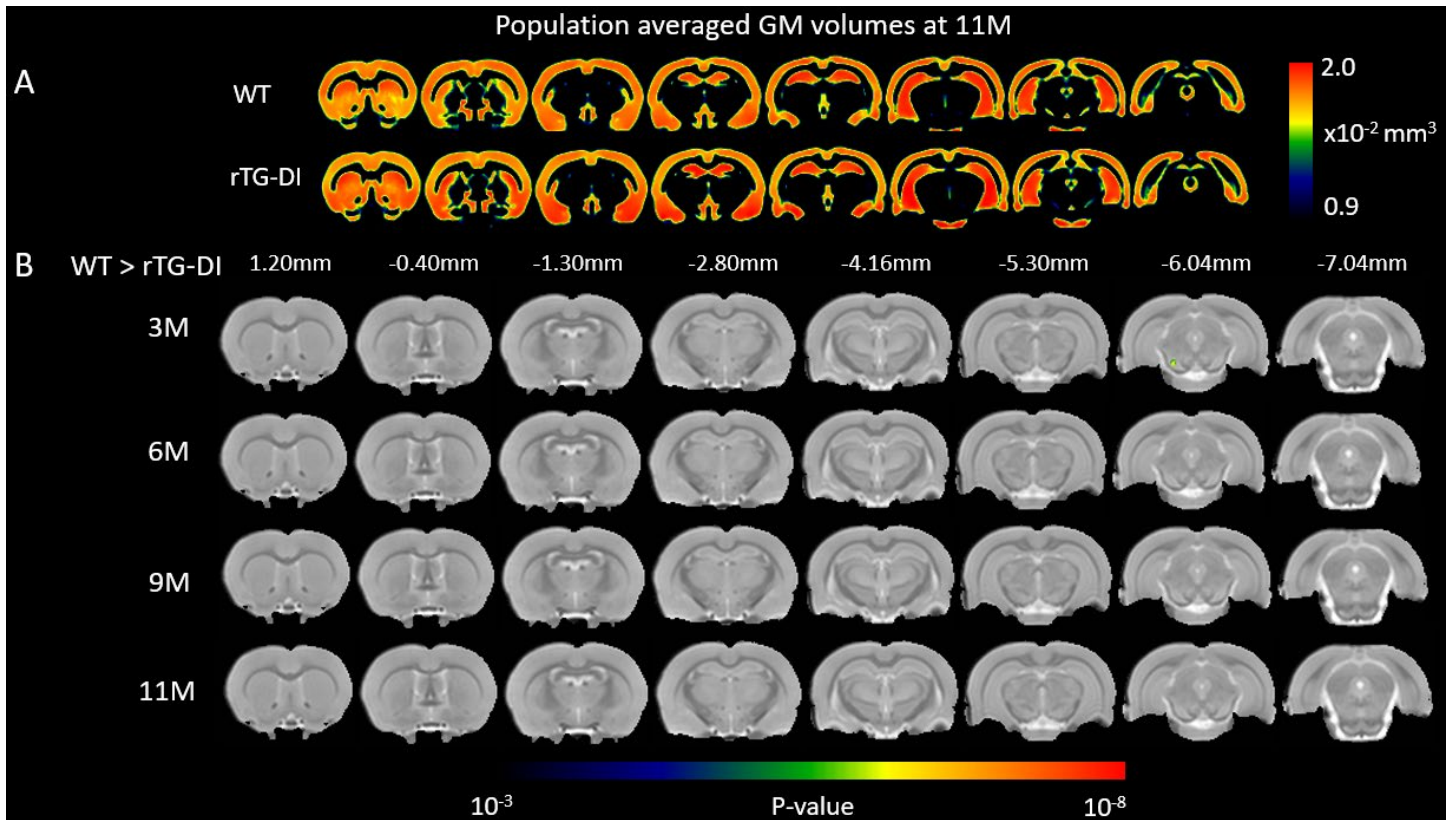


### Supplementary Figure 2: Delineation of regions of interest using tractography

**A:** Tractography guided manual delineation of corpus callosum (CC), anterior commissure (AC), and frontal cortex (FC) are shown. **B:** Streamlines represent population averaged and direction encoded fiber tracts within each region of interest (ROI). The arrows indicate the direction of color encoding. **C:** Streamlines represent population averaged and FA weighted fiber tracts within each region of interest (ROI).

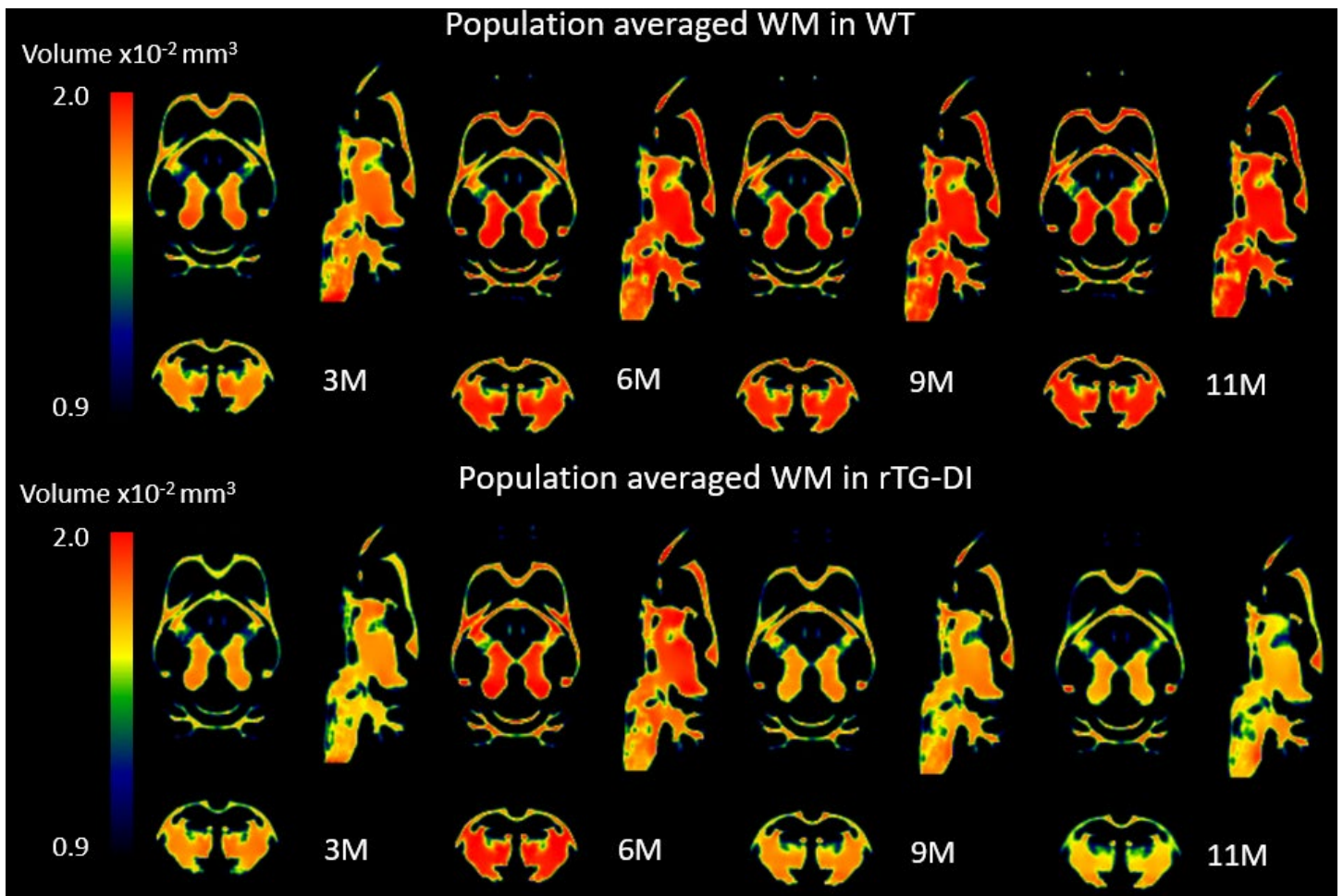


**Supplementary Figure 3: Blood oxygen saturation (top) and heart rate (bottom) parameters measured continuously in the rats during the four different MRI scanning sessions.**



**Supplementary Figure 4: Voxel-wise GM morphometry comparison between rTg-DI and WT rats documented *in vivo***

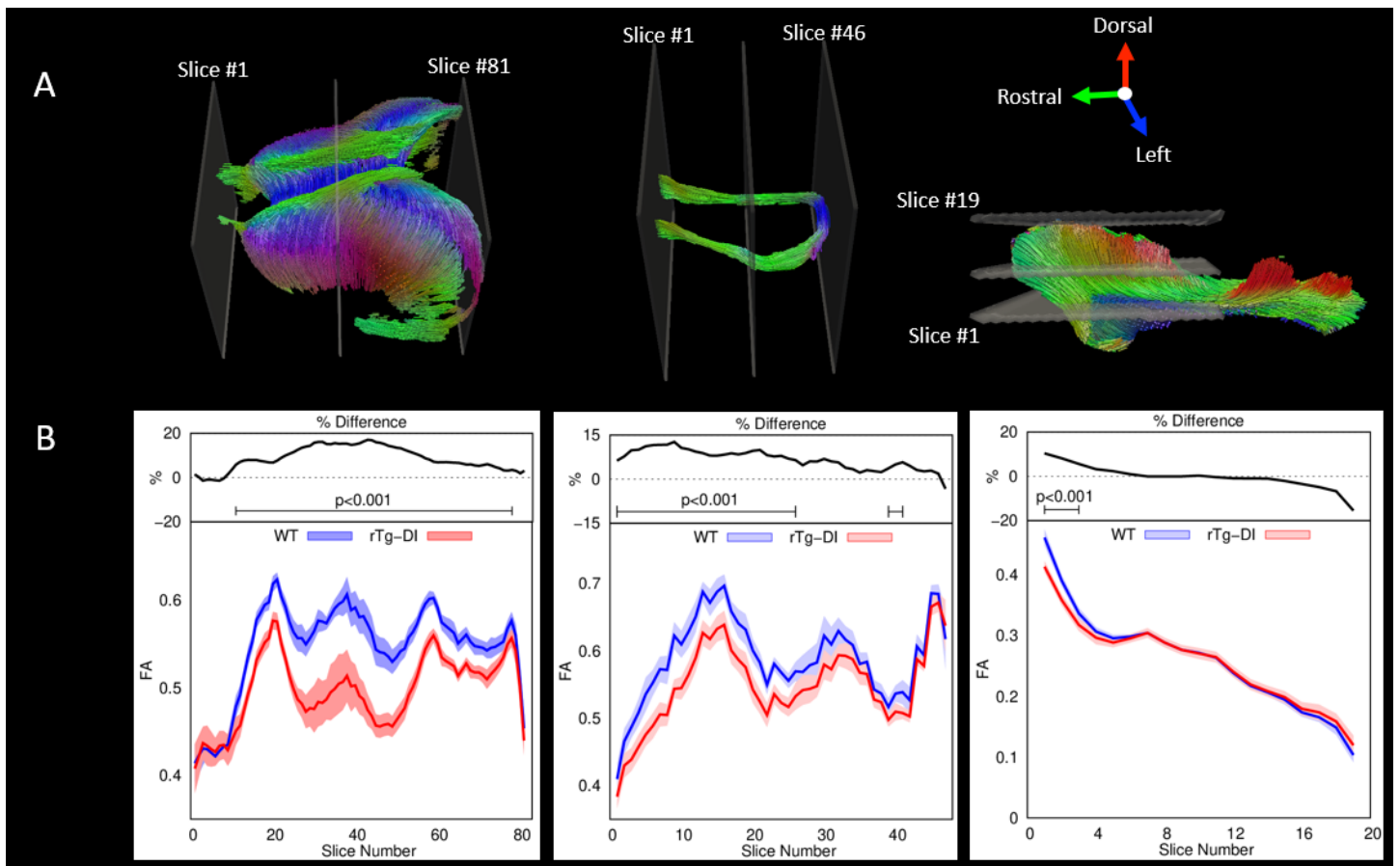
The proton density weighted (PDW) MRI acquired *in vivo* was used for quantitative assessment of GM loss. **A:** Spatially normalized population averaged GM volumetric maps of 11M old rTg-DI and WT are shown in color maps. **B:** For each age group, statistical parametric maps (color coded for p-values) were calculated, corrected for multiple comparison at FDR < 0.05, and overlaid onto the population averaged PDW MRI images to display anatomical areas. Anatomical levels of the axially displayed anatomical templates are given by their nearest Bregma distance.



**Supplementary Figure 5: Population averaged WM volume maps documented *in vivo***

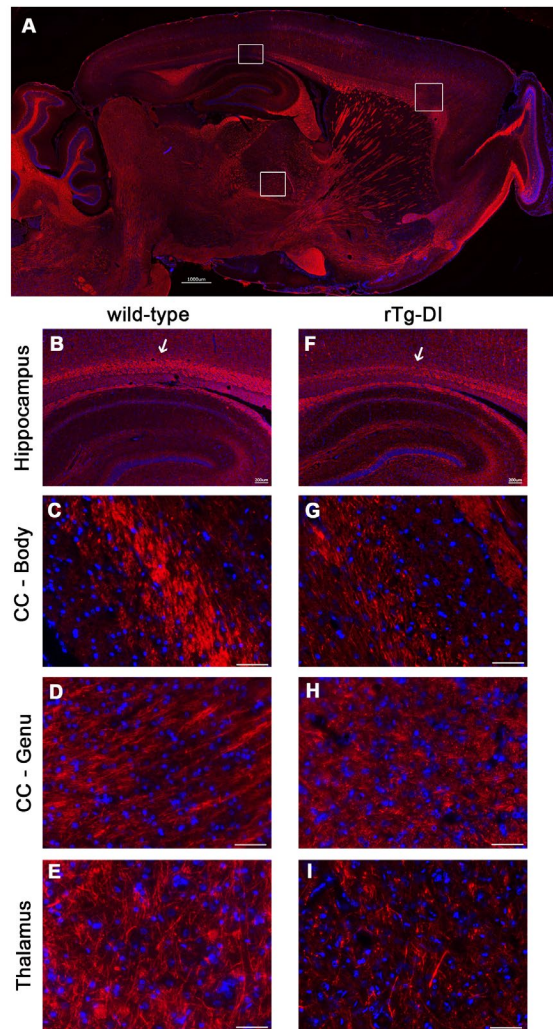
Population averaged whole brain WM volumetric maps of WT (N=11) and rTg-DI (N=11) at 3M, 6M, 9M and 11M of age are shown. For each animal, a deformation field derived from the DARTEL spatial registration was applied onto a WM segmented image in native space for spatial normalization. Spatially normalized WM maps were further modulated by Jacobian determinant to preserve the total brain volume and population averaged.





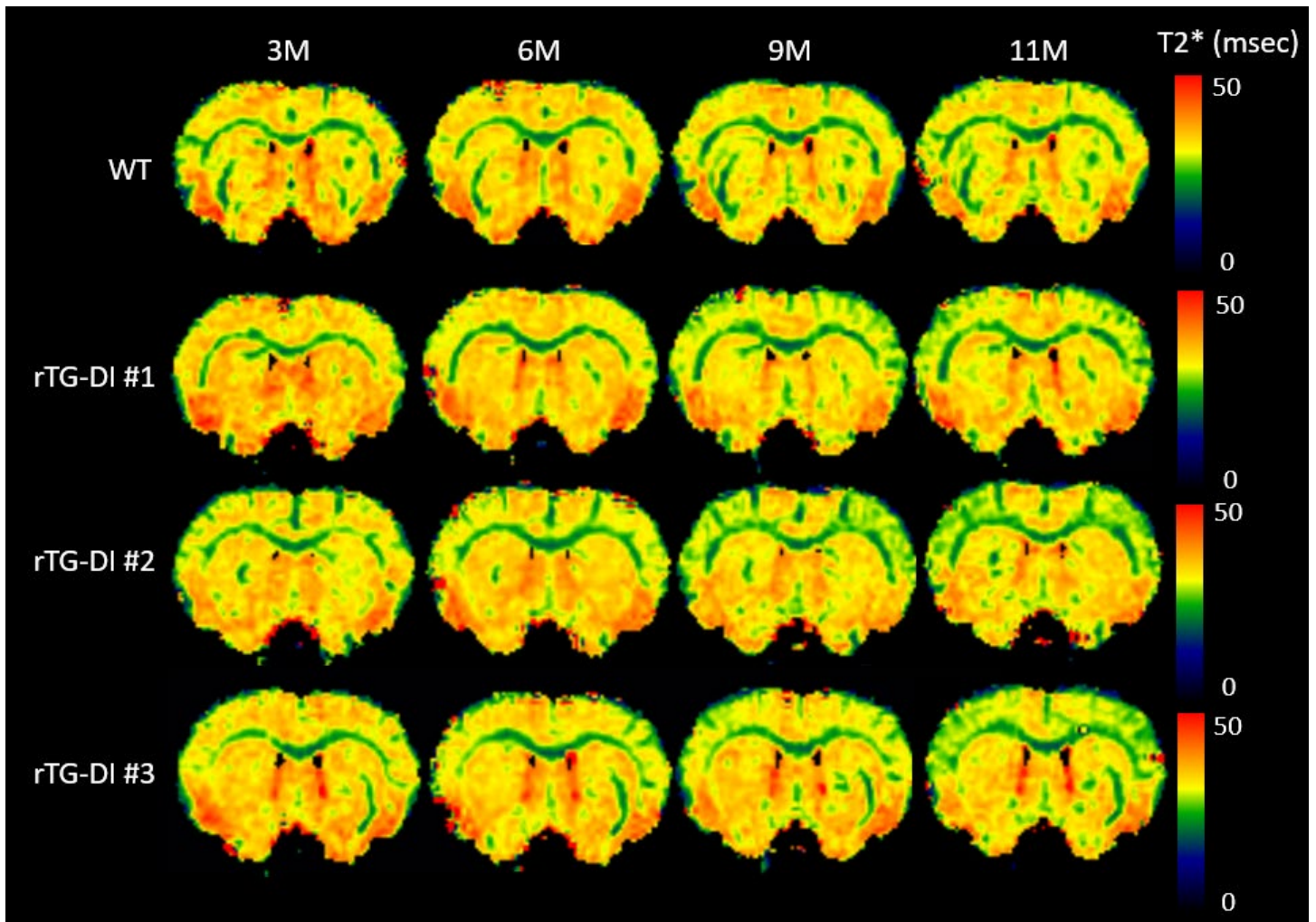
**Supplementary Figure 6: DTI based tractography of WM tract differences between WT and rTg-DI strains**

**A:** Direction encoded tractography in the corpus callosum (CC) (left), anterior commissure (AC) (middle), and projection fibers from corpus callosum to frontal cortex (FC) (right) are shown. Arrows indicate the direction of color encoded tracts. Rectangular panels represent image planes used for calculating 2D FA slice profiles in each structure. **B:** Mean (solid lines) and standard deviation (SD) (shaded) of FAs within each slice are plotted as a function of slice. % differences (solid white lines) between rTg-DI and WT rats in each slice were plotted above the FA slice profile. Significant differences between the two groups revealed by t-test were shown in solid lines below the percent differences ( $p$ -value  $< 0.001$ ).



### Supplementary Figure 7: Axonal loss and fragmentation in rTg-DI rats validated by histology

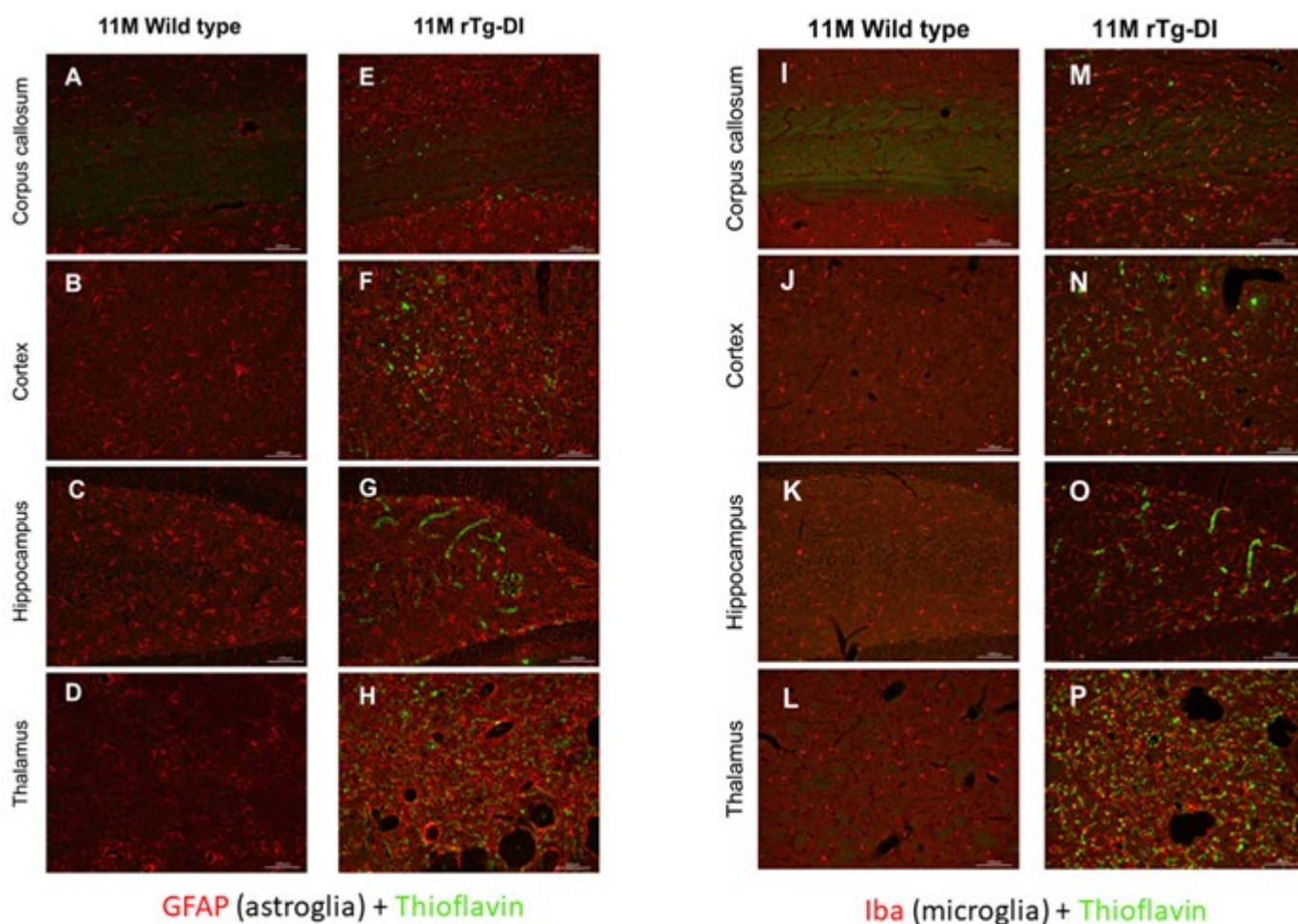
A: Representative sagittal section from a 11 month (M) old rTg-DI rat immunolabeled for axons using the pan-axonal neurofilament marker SM312 and DAPI. The three white boxes highlight the anatomical locations presented in the panels below: Corpus callosum (CC) body above the dorsal hippocampus, CC-Genu and the thalamus. The left panel set shows representative images of the dorsal hippocampus and the three preselected regions from a 11M old WT rat (B-E) and an 11M old rTg-DI rat (F-I). Thinning of the body of the CC above the dorsal hippocampus is noted in the 11M rTg-DI rat (F arrow, G) compared to the 11M WT (B arrow, C). Decreased labeling of axons signifying general axonal loss was evident throughout the CC of the 11M rTg-DI rat (G). At the level of the genu, disruption of the axonal labeling is evident and the axonal segments appear fragmented in the rTg-DI rat (H) compared to the WT rat (D). In the thalamus, labeling of axons is strikingly reduced in the 11M rTg-DI rat (I) compared to WT (E). (A) scale bar = 1000  $\mu$ m; (B, F) scale bars = 200  $\mu$ m; (C-E) and (G-I) scale bars = 50  $\mu$ m.



**Supplementary Figure 8: T2\* hypointensity in cortices documented *in vivo***

Representative spatially normalized T2\* map of one WT rat and three rTg-DI rats at 3M, 6M, 9M and 11M of age are displayed axially at 0.48 mm Bregma distance. In WT, T2\* maps appear similar and reproducible across all time points. Three cases of rTg-DI rats indicate the T2\* hypo-intensities in cortex, which appear as diffuse or columns, emerged at 9M which then progressively became more conspicuous over time.





### Supplementary Figure 9: Perivascular neuroinflammation in 11M rTg-DI rats

Pronounced perivascular neuroinflammation in 11M rTg-DI rats (E-H and M-P) compare to WT rats (A-D and I-L) was evident in the form of astrogliosis (GFAP in red) and activated microglia (Iba-1 in red) in regions with heavy perivascular fibrillar A $\beta$  burden (green) such as the thalamus and hippocampus in comparison to WT.

Scale bars = 100  $\mu$ m.

### Supplementary method:

#### Immunohistochemical analyses:

Fixed rat brain tissues obtained from the MRI studies were cut in the sagittal plane at 10-12  $\mu$ m thickness using a Leica RM2135 microtome (Leica Microsystems Inc., Bannockburn, IL), placed in a flotation water bath at 40°C, and then mounted on Colorfrost/Plus slides (Fisher Scientific, Houston, TX). Antigen retrieval was performed by treating the tissue sections with proteinase K (0.2 mg/ml) for 10 min at 22 °C. Primary antibodies were detected

with Alexa Fluor 594-conjugated donkey anti-rabbit or Alexa Fluor 488-conjugated goat anti-mouse secondary antibodies (1:1000). Staining for fibrillar amyloid was performed using thioflavin S. The following antibodies were used for immunohistochemical analysis: mAb66.1 (1:250), which recognizes residues 1-5 of human A $\beta$  [1]; rabbit polyclonal antibody to collagen type IV to visualize cerebral microvessels (1:100; ThermoFisher, Rockford, IL); rabbit polyclonal antibodies to GFAP (1:200; Dako, Santa Clara, CA) and Iba-1 (1:200; Fujifilm Wako Pure Chemical, Osaka, Japan) for detection of astrocytes and microglia, respectively. Prussian blue iron staining was performed to detect hemosiderin deposits reflecting signs of previous microhemorrhage. [1] Von Kossa calcium staining was used to detect small vessel occlusion/calcifications in the brain. [2] The percent area amyloid coverage of cerebral microvessels in the different brain regions and the percent area iron staining in the thalamic region were determined using stereological principles as described.[3]

Evaluation of axonal integrity in different brain regions and corpus callosum WM volume and myelin basic protein (MBP) levels in 11-12M old rTg-DI and WT rats were carried out in a separate series of rats not used for MRI. For analysis of axonal integrity rat brain tissue sections were immunolabeled with antibody SM312 pan axonal neurofilament marker (1:250; BioLegend, San Diego, CA) and nuclear staining was performed with 4',6-diamidino-2-phenylindole (DAPI, 10236276001, Sigma-Aldrich).

To determine the corpus callosum volume in WT and rTg-DI rats fresh frozen brain sections were cut at 12  $\mu$ m thickness in the sagittal plane spanning the entire brain hemisphere. Every 4<sup>th</sup> section was selected and stained for myelin using the Black Gold II Myelin Staining Kit according to manufacturer's protocol (AG105; MilliporeSigma, Burlington, MA). Stitched images of the sagittal brain sections were prepared using a Keyence BZ-X710 microscope. The corpus callosum was outlined and the area was measured and calibrated with BZ-X analyzer software. Then the volume of main corpus callosum (from lateral 0.5 mm to lateral 2.66 mm) was calculated based on the area multiplied by the thickness.

For measurement of MBP levels in the corpus callosum sagittal sections at 25  $\mu$ m thickness were prepared from fresh frozen WT and rTg-DI rat brains, mounted on Leica Frame Slides (Leica Microsystems, Danvers, MA) and the corpus callosum from each section was identified, excised and captured using a LMD6 laser capture microdissection microscope (Leica Microsystems). Collected tissue samples were lysed in RIPA buffer via

sonication (12 x 1 sec bursts) on ice, followed by 1 h incubation on ice. Protein concentrations of each sample were determined by the BCA method and normalized. Sufficient 2× SDS sample buffer (2 % (w/v) SDS, 0.01 % (w/v) bromphenol blue, 20 mM DTT, 50 mM Tris-HCl, pH6.8) was added to each sample, resolved via SDS-PAGE and transferred to polyvinylidene difluoride (PVDF) membrane (Imobilon-FL, EMD Millipore, Billerica, MA) for immunoblotting. MBP was detected using affinity-purified goat polyclonal antibody [4] (1:500) and  $\beta$ -actin was detected using a mouse monoclonal anti- $\beta$ -actin antibody (1:5000; A5441, Sigma). Immunoblots were then probed with species-specific horseradish peroxidase (HRP)-conjugated secondary antibodies and HRP-catalyzed chemiluminescent signal was revealed using ECL Western Blotting Substrate (32106, ThermoFisher) and detected using an Odyssey Fc imager (LI-COR Biosciences, Lincoln, NE). Signal intensity was measured using ImageJ software (NIH), and the MBP signal in each lane was normalized against its corresponding  $\beta$ -actin signal.

## References

- [1] Deane R, Du Yan S, Subramanian RK, LaRue B, Jovanovic S, Hogg E *et al.* RAGE mediates amyloid-beta peptide transport across the blood-brain barrier and accumulation in brain. *Nat Med* 2003; 9(7): 907-13.
- [2] Rungby J, Kassem M, Eriksen EF, Danscher G. The von Kossa reaction for calcium deposits: silver lactate staining increases sensitivity and reduces background. *Histochem J* 1993; 25(6): 446-51.
- [3] Long JM, Kalehua AN, Muth NJ, Hengemihle JM, Jucker M, Calhoun ME *et al.* Stereological estimation of total microglia number in mouse hippocampus. *J Neurosci Methods* 1998; 84(1-2): 101-8.
- [4] Ou-Yang MH, Xu F, Liao MC, Davis J, Robinson JK, Van Nostrand WE. N-terminal region of myelin basic protein reduces fibrillar amyloid-beta deposition in Tg-5xFAD mice. *Neurobiol Aging* 2015; 36(2): 801-11.